3D QSAR, Molecular Docking, and ADMET Studies of a Series of 2-Acetylphenol-Rivastigmine Hybrids against Monoamine Oxidase A Inhibitors

L. Naanaai*, A. El Aissouq, H. Zaitan and F. Khalil

Laboratory of Processes, Materials, and Environment (LPME), Faculty of Science and Technology, Sidi Mohamed Ben Abdellah University, Fez, Morocco

In this study, a number of 2-acetylphenol-rivastigmine hybrids were rationally designed as drugs for the treatment of behavioral disorders, especially depression. A series of 2-acetylphenol-rivastigmine hybrids against monoamine oxidase A (MAO-A) inhibitors were identified using *in-silico* virtual screening studies, such as three-dimensional (3D) QSAR, molecular docking, and pharmacokinetic properties (absorption, distribution, metabolism, excretion, and toxicity (ADMET)). This was done to obtain new ligands with high inhibitory activities. The best 3D-QSAR model was developed using the partial least squares approach and comparative molecular similarity index analysis (CoMSIA). The developed model demonstrated strong correlative and predictive capabilities ($r^2 = 0.904$, $q^2 = 0.699$, and SEE = 0.094). The changes in the biological activity of four main components were significantly influenced by the steric, electrostatic, hydrophobic, and H-bond acceptor sites. The results were used to analyze the newly developed molecules using in-silico drug-likeness, ADMET, and molecular docking.

INTRODUCTION

The mitochondria-related enzyme monoamine oxidase (MAO) is highly expressed in intestinal and neural tissues. MAO-A and MAO-B are the two isoforms of the enzyme. Despite their high sequence similarity, the substrate-inhibitor recognition and tissue distribution of these isoforms vary. Although the sequence similarity between the two isoforms of MAO-A and MAO-B is 73%, they differ primarily in their inhibitor selectivity, substrate specificity, and tissue distribution [1-3]. The unique substrate properties of MAO-A include a greater number of endogenous amines, such as norepinephrine, serotonin, and epinephrine. In addition, the functional polymorphism of the MAO-A gene and the somatostatin signaling pathway were found to be associated with depression [4-5].

Some recent studies have attempted to synthesize new

compounds as inhibitors of the MAO-A enzyme. Shalaby *et al.* studied chalcone derivatives using Claisen-Schmidt condensation and their inhibitory effects on human MAO-A [6]. Kumar *et al.* synthesized novel 4,6-diphenylpyrimidine derivatives and evaluated MAO-A [7]. Furthermore, Turan-Zitouni *et al.* designed and synthesized a series of new N-pyridylhydrazone derivatives and evaluated them for their inhibitory activity against both MAO isoforms [8]. In another study, using recombinant human MAO-A, Larit *et al.* extracted the pure chemicals myricetin, quercetin, and genistein from the plants Cytisus villosus and Hypericum afrum, respectively [9]. Lee *et al.* isolated alternariol monomethyl ether (AME), a dibenzopyrone derivative, and altertoxin II from Alternaria brassicae. AME has been reported to be a very potent and selective inhibitor of human MAO-A [10]. Other studies have been carried out on hybrids using a combination of molecules and acetylphenol as well as rivastigmine with the aim of developing drugs for patients with Alzheimer's disease [11-16].

In recent years, developed bioinformatic methods,

---

*Corresponding author. E-mail: lhoucine.naanaai@gmail.com

particularly in molecular modeling, have become an integral part of a large number of techniques, including *in-silico* screening, two- and three-dimensional (3D) QSAR, absorption, distribution, metabolism, excretion, and toxicity (ADMET), and molecular docking [17-23], used in the search for new molecules for therapeutic purposes [17]. The 3D-QSAR relies on the relationship between biological activity and molecular descriptors. In addition, comparative molecular similarity analysis (CoMSIA) has been used extensively to find the correlation between the biological activity of molecules and their 3D structures. Molecular docking is an effective way to both predict an optimized ligand structure at a receptor binding site and study the interaction between the receptor and the ligand [24]. Thus, a combination of 3D-QSAR and molecular docking may provide us with specific inhibitors and receptors.

In the present study, 3D-QSAR and molecular docking were used to perform a molecular modeling study on a set of acetylphenol-rivastigmine hybrids. The IC_{50} values of the selected compounds, designated as selective inhibitors for the enzyme MOA, varied from 5.7 to 42.1 μM. After newcompounds with high biological activities were designed using the developed mathematical model, their pharmacokinetic characteristics were examined using the in-silico ADMET profile.

MATERIALS AND METHODS

Data Set

The data related to the 25 molecules used in this study were obtained from the literature [25]. The information on inhibitory activity is presented as an IC_{50} value. IC_{50} values were converted to pIC_{50} using the following equation: $pIC_{50} = -logIC_{50}$. In the CoMSIA model, the data set was divided into a training set (20 molecules) and a test set (5 molecules). The structures of the compounds and their related inhibitory activities are shown in Table 1, where pIC_{50} values for the 25 inhibitors range from 4.38 to 5.25.

Table 1. The 25 Designed Compounds and the Data Related to Their Observed Activities, Predicted Activities, and Residual Values Generated by 3D-QSAR

Compound	Structure	IC_{50}	pIC_{50} (Observed)	pIC_{50} (Predicted)	Residual
3a		7.1	5.15	5.04	0.11
3b		7.8	5.11	5	0.12
3c*		7.3	5.14	5.03	0.11
3d		13.7	4.86	4.89	-0.02

Table 1. Continued
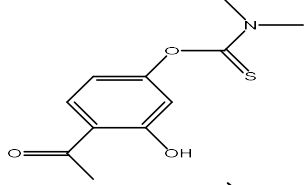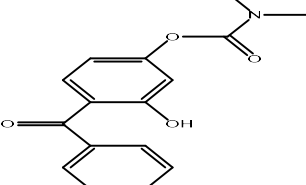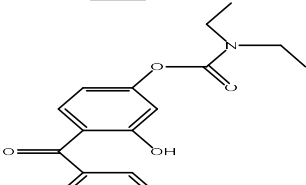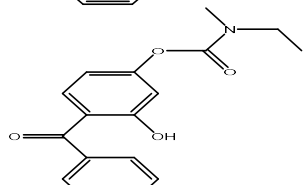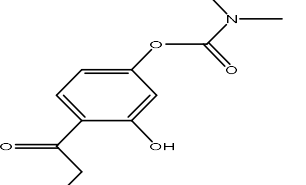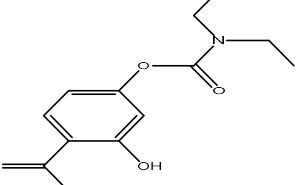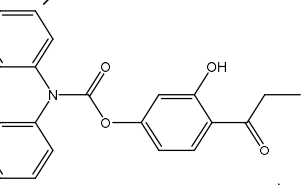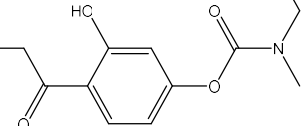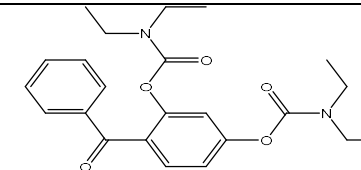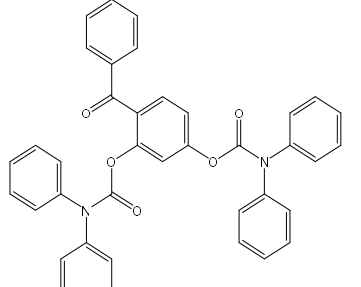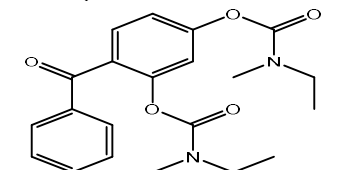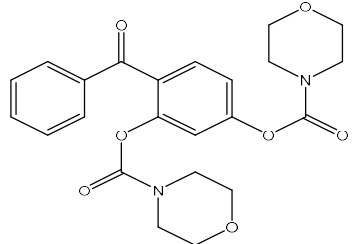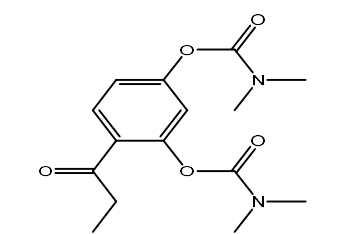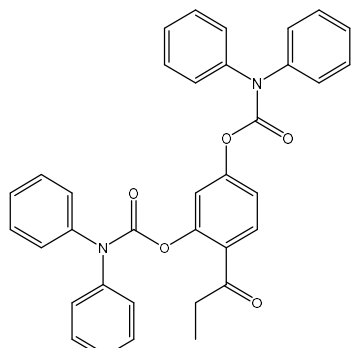
3e		5.7	5.25	5.1	0.15
3f		11.3	4.95	5.05	-0.09
3g*		9.6	5.02	5	0.02
3h		9.2	5.04	5.02	0.03
3i		15.3	4.82	4.94	-0.12
3j		17.9	4.75	4.9	-0.14
3k		13.4	4.87	4.81	0.07
3l		12.1	4.92	4.91	0.01

Table 1. Continued

3m*		19.5	4.71	4.71	0.00
3n		11.4	4.94	5	-0.06
4a*		30.1	4.52	4.67	-0.15
4b		19.7	4.71	4.74	-0.02
4c		36.2	4.44	4.56	-0.12
4d		39.7	4.4	4.44	-0.04
4e*		33.4	4.48	4.45	0.03

Table 1. Continued

4f	42.1	4.38	4.37	0.02
4g	29.7	4.53	4.56	-0.02
4h	32.6	4.49	4.41	0.09
4i	35.9	4.44	4.46	-0.01
4j	28.2	4.55	4.51	0.04
4k	20.8	4.68	4.63	0.05

Note. * = Test set molecules.

Alignment of Database and Molecular Modeling

As shown in Fig. 1a, the compounds were aligned based on the common substructure. The molecular modeling and alignment of compounds, as illustrated in Fig. 1b, were carried out using SYBYL-x 2.0 Tripos software [26]. The 3D molecular structures were sketched using the Chem3D software. The energy of each molecule was minimized using the Tripos force field in SYBYL and Gasteiger-Hückel charges [27]. For the energy minimization, the maximum number of interactions was set to 2000. Energy minimization was achieved when the energy convergence criterion reached 0.05 kcal mol^{-1}.

CoMSIA Setup

A probe atom with a charge of +1.0, a radius of 1.0 Å, and hydrophobic and hydrogen bonding interactions was used to calculate the following CoMISA descriptors: steric field, electrostatic field, hydrophobic field, hydrogen-bond acceptor, and hydrogen-bond donor [28]. At each grid intersection evenly spaced apart with 1 space and extended up to 4, the attenuation factor used had a default value of 0.3 [29].

Model Validation and Regression Analysis

CoMSIA descriptors and pIC$_{50}$ appeared to be linearly correlated under the partial least squares (PLS) approach. The independent variables used were CoMSIA descriptors. In the cross-validation procedure, the threshold column filtering was set to 2.0 kcal mol^{-1}. To perform the leave-one-out cross-validation (LOO-CV), one molecule from the data set was removed. Then, using a model developed from the remaining data, the activity of the removed molecule was predicted. The validity of the resulting model was tested using the LOO-CV, and the optimal number of components (ONC) was determined. The number of components that resulted in the highest (r^2) correlation coefficient (r^2_{cv}) following cross-validation was chosen as the ONC. Finally, the CoMSIA model was developed using the PLS approach without cross-validation but with the ONC being determined by cross-validation.

The predictive ability of the 3D-QSAR models was validated by predicting the activities of a test set of 5 molecules that were not included in the training set. These compounds were aligned to the model, and their pIC50 values
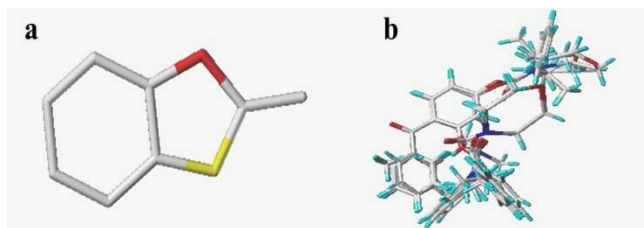

Fig. 1. (a) Common substructure (b) Molecular alignment of all molecules in the data set.

were predicted by the model developed using the training set.

Lipinski's Rule and ADMET Prediction

Lipinski's Rule and ADMET properties for different physicochemical descriptors and pharmaceutically relevant compounds were performed using the pkCSM web server [30]. This approach has been widely used as a screening method for molecules that are likely to be developed in drug design studies. The use of ADMET descriptors allowed us to remove molecules with unfavorable ADMET profiles to avoid costly reformulation in the future. Furthermore, some structural modifications proposed to optimize ADMET parameters were considered before investing resources in synthesis.

Molecular Docking

In this study, molecular docking was used to perform a molecular modeling study on a set of acetylsphenol-rivastigmine hybrids to determine the type of interactions between the receptor (PDB code: 2bxr) and the ligand. First, the X-ray crystal structure of the receptor was downloaded from the RCSB protein data bank (http://www.rcsb.or/pdb/). After water molecules were removed, polar hydrogens were added to the receptor. A coordinate grid (X = 32297, Y = 4814, and Z = 7434) was plotted at the catalytic site of the MAO-A enzyme, and AutoDock tools were used to perform molecular docking. The binding pocket was validated by the redocking protocol, and the details are presented under the "Materials and Methods Section": molecular docking with the root-mean-square deviation = 0.3 Å (Fig. 2). Finally, the molecules in the prepared dataset were docked to the active site of the 2bxr using AutoDock Tools and AutoDock Vina [31], and the 3D structures were visualized using PyMol and Discovery Studio 2020.
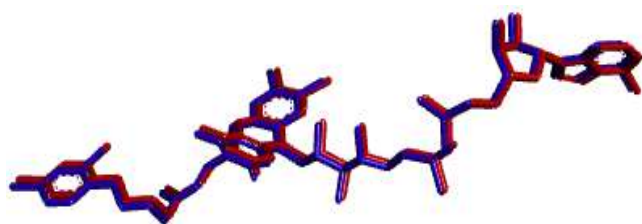
Fig. 2. The superposition of the co-crystallized ligand (red) and the redocked ligand (blue).

RESULTS AND DISCUSSION

CoMSIA Model

The CoMSIA model was used to construct a 3D-QSAR model for novel 2-acetylphenol-rivastigmine hybrids as MOA inhibitors for the treatment of depression. The principal model was obtained using a combination of four descriptors: steric fields, electrostatic fields, hydrogen-bond donor, and hydrophobicity. The CoMSIA model had a positive effect on the inhibition efficiency, and a q^2 cross-validation of 0.69 was calculated for the four optimal components. PLS analysis without cross-validation yielded the conventional r^2 value of 0.9, F value of 33.57, and a standard error of estimate of 0.09. The test r^2 score of 0.9 calculated by the model was higher than 0.5, indicating that the CoMSIA model could make accurate predictions. The contribution of steric fields, electrostatic fields, hydrogen-bond donor, and hydrophobicity were 13%, 27%, 42%, and 18%, respectively. Thus, these results indicate that the predominant descriptor in the CoMSIA model was the hydrogen-bond donor.

Table 1 shows the predicted pIC_{50} values and residual values (the difference between predicted and experimental values) for several molecules in the combined training and test phases using the best CoMSIA model. The results of the CoMSIA model are presented in Table 2. Figure 3 shows the correlation between the experimental activity of the training (blue dots) and test (red dots) sets predicted using the PLS approach.

CoMSIA Contour Maps

In Fig. 4, the green contours represent the steric field, which indicates areas where the presence of non-bulky
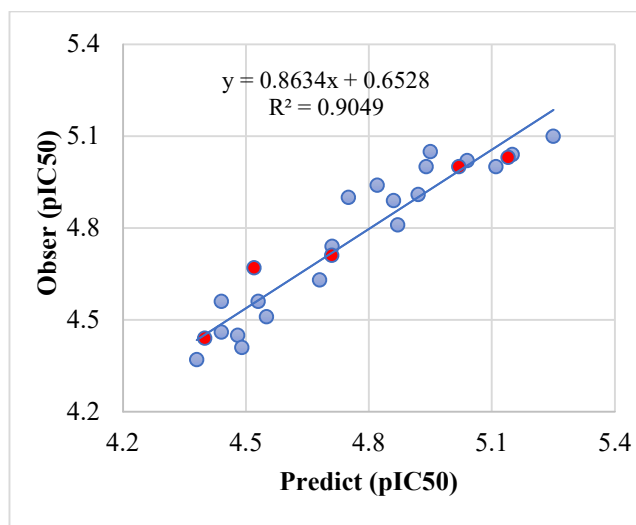
Fig. 3. The correlation between the training (blue dots) and test (red dots) sets experimental activity predicted using the PLS approach.

Table 2. The Statistical Factors of the CoMSIA Model

Statistical factors	CoMSIA
N	4
q^2_{LOO}	0.69
r^2	0,90
SEE	0.09
F_{Value}	33.57
r^2_{test}	0.85
Contributions	-
Electrostatic	18%
Hydrophobic	27%
Donor	42%
Acceptor	-
Steric	13%

Note. N = the optimal number of components; q = LOO-CV; r^2 = cross-validation coefficient; SEE = standard error of estimate; r^2_{test} = correlation coefficient; F = Fischer's value.

(a) Steric fields

(b) Electrostatic fields

(c) Hydrophobic fields

(d) Hydrogen bond donor contour map
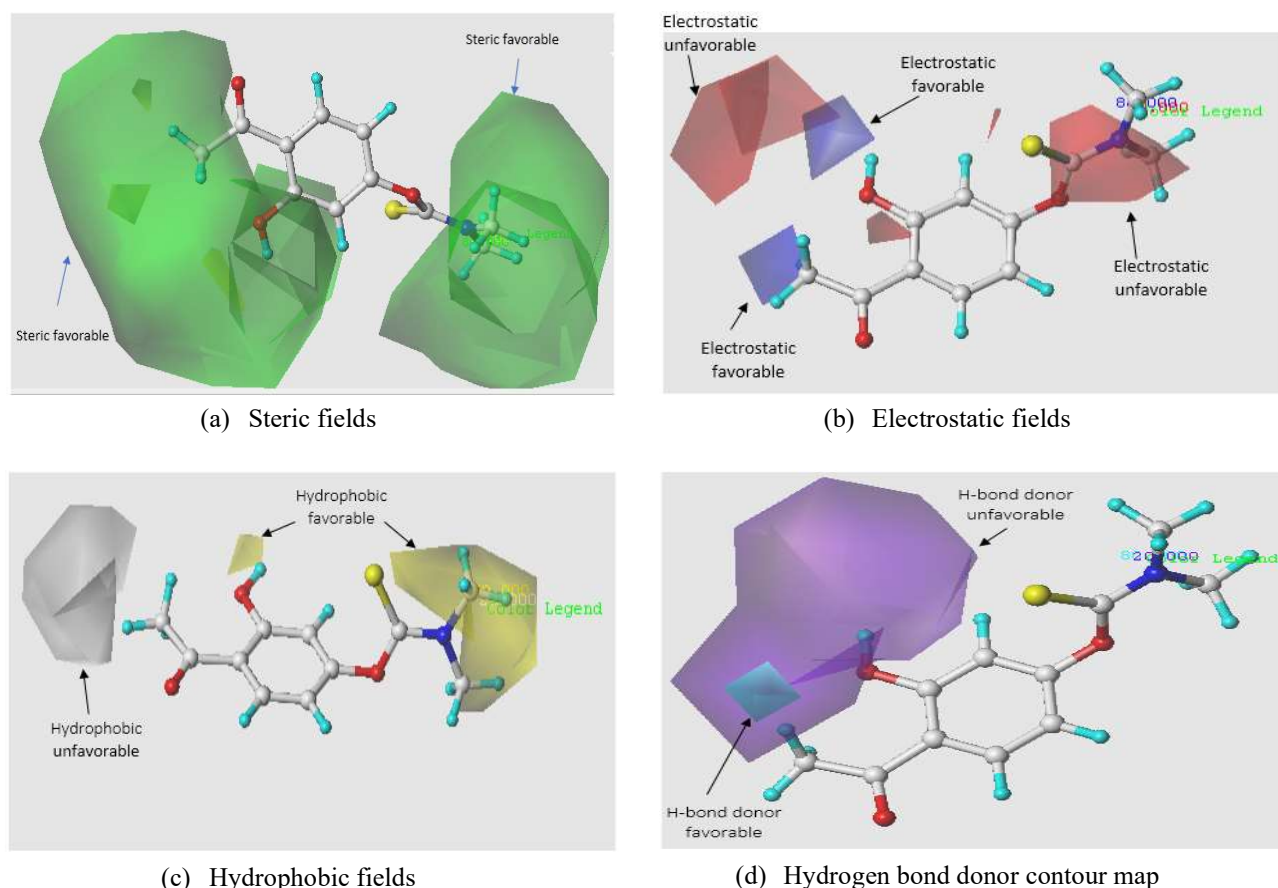
Fig. 4. The best contour map for the CoMSIA model using 3E as a template molecule.

groups is encouraged, which increases the inhibitory activity of the molecules. Based on Fig. 4a, the presence of the green contours at the R, R^1, and R^2 positions suggests that a less dense cluster in this area would be advantageous. When all the compounds modified by R^1 and R^2 were checked while keeping the position R (R = CH$_3$) constant, it was found that derivatives 3a, 3c, and 3b had the following order of inhibitory activity: 3a (R^1 = CH$_3$, R^2 = CH$_3$) > 3c (R^1 = CH$_3$, R^2 = C$_2$H$_5$) > 3b (R^1 = C$_2$H$_5$, R^2 = C$_2$H$_5$).

When the compounds were modified by R^1 and R^2, and the R position (R = Ph) was kept constant, the 3f, 3g, and 3h had the following order of inhibitory activity: 3f (R^1 = CH$_3$, $R^2$ = CH$_3$) > 3g (R^1 = C$_2$H$_5$, R^2 = C$_2$H$_5$) > 3h (R^1 = CH$_3$, R^2 = C$_2$H$_5$). Compared to the target compounds 3a-3n with monosubstituted carbamates, the target compounds 4a-4k with bis-substituted carbamates indicated poor MAO-A

inhibitory activity, suggesting that the hydroxy group was critical in MAO inhibition. Additionally, the carbamate moiety was observed to have no clear effect on the MAO-A inhibitory efficacy.

The blue and red contours in Fig. 4b represent the electrostatic field, which shows areas where the electron donor and acceptor groups would be advantageous, respectively. In the electrostatic field, two blue contours around the extremity of R and a red contour in the vicinity of the substituents R^1 and R^2 demonstrated that the electron-attracting substituents in the vicinity of R1 and R^2 and electron-donating substituents at the extremity of R were crucial for the inhibitory activity of the compounds. The strong electron-attracting carbamothioate group around the electron-donating R^1 and R^2 groups (-CH$_3$, -C$_2$H$_5$) led to a significant increase in the inhibitory activity of these

compounds.

It is possible to show which regions prefer hydrophobic and hydrophilic properties by identifying the yellow and white contours in hydrophobic fields. The yellow contour around the chain in positions R1 and R^2 in Fig. 4c suggests that a hydrophobic substituent would be advantageous for the inhibitory activity whereas a large white contour toward the extremity of R indicates that a hydrophile group may be preferred.

The cyan outline represents a favorable group of hydrogen-bond donors in the hydrogen bond site. The cyan contour around the site of the group (OH) in Fig. 4d shows that the groups with a hydrogen bond may be beneficial for inhibitory activity. In fact, the (OH) group served as a hydrogen-bond donor in this position.

Designing of New Molecules

Once the output of the 3D-QSAR model was interpreted, and the descriptors that strongly influenced the inhibitory activity were identified by the analysis of the maps, some modifications were made to the active molecule 3E through the substitution of R^1, R^2, and R. Using the most active molecule (3E) as a template, the newly predicted ligands were improved and aligned to the database. These potential medications exhibited more biological activities than molecule 3E. Table 3 represents the structure and activity of each predicted molecule. Figure 5 captures the strategy followed to design the new molecules.

Lipinski's Rule and ADMET Properties

The relevant Lipinski's rule parameters, such as molecular weight, number of hydrogen bonds (donor and acceptor), number of rotational bonds, and logP, are presented in Table 4. There were no deviations from Lipinski's rule of 5 for any of the compounds. The logP must be greater than zero and less than three ($0 < logP < 3$) to have a good oral biodisponibility. The medication had poor water solubility due to an excessively high logP value. Moreover, the medication had trouble penetrating the lipid bilayers of cell membranes due to the very low logP values.

In this study, we focused primarily on the following three properties:
- Human intestinal absorption properties (HIA) to estimate the percentage of substances absorbed by the human small
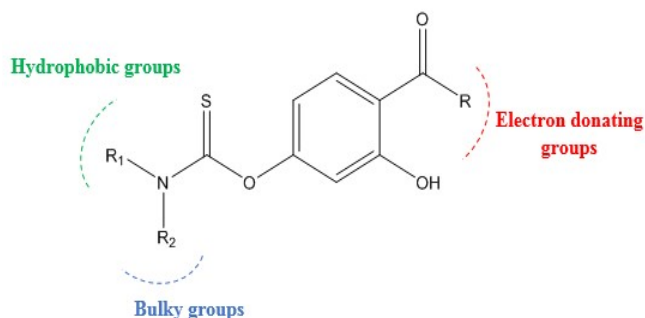

Fig. 5. The strategy followed for the design of new molecules.

intestine. In fact, a molecule with an absorbance of less than 30% was considered poorly absorbed;
- The *in vitro* CaCO-2 cell permeability to estimate the absorption of orally administered drugs. According to the pkCSM prediction model, high CaCO-2 permeability corresponds to predicted values above 0. 90;
- The *in vivo* penetration of the blood-brain barrier (BBB) to confirm the ability of a substance to pass into the brain. A substance is expected to cross the blood-brain barrier easily if the logBB value is greater than 0.3 whereas substances with logBB less than -1 are poorly distributed in the brain. Other properties predicted included cytochrome P450 inhibition and substrate, water solubility (logM), total clearance, and toxicity.

Table 5 shows the results of the ADMET properties of the predicted molecules. Based on the results, all of the chosen Pred 1-7 compounds had a suitable pharmacological profile. Furthermore, the blood-brain permeability values of all substances were acceptable. This indicates that in order for a medicine to enter the central nervous system and move through the brain, the above-mentioned molecules appear to be the most crucial factor. A negative Ames test revealed that the studied derivatives (Pred 1-7) were not toxic. The hepatotoxicity testing showed that none of the molecules were toxic.

Molecular Docking

Molecular docking was primarily designed to predict the structure of the complex that resulted from the interaction between an active molecule and a protein (receptor). First, the active site was determined by extracting the native ligand

Table 3. Structures and Predicted pIC50 Activity (Pred) Based on the 3D-QSAR Model of Predicted Compounds

N°	Structure	pIC_{50} (Pred)
Pred1		5.275
Pred2		5.295
Pred3		5.308
Pred4		5.337
Pred5		5.385
Pred6		5.387
Pred7		5.404

from its PBD structure (PDB code: 2bxr). It was established that the designed molecules (pred 1-7) had a minimum binding energy between -7.90 and -9.70 kcal mol^{-1}. When the resultant complex was compared with the reference ligand (-7.90 kcal mol^{-1}), it was found that all complexes generated by the proposed compounds and the MAO-A receptor were more stable. Table 6 represents the binding energy of the predicted compounds as well as their interactions with the MAO-A enzyme.

Figure 6 shows that the proposed molecules interacted with the monoamine oxidase A enzyme *via* multiple interactions. The compounds (Pred 1-7) showed a similar pattern of hydrogen interactions with the amino acid residues Arg 33, Gly 32, and Met 395. In addition, some hydrophobic interactions were observed with Arg 33, Ala 398, Tyr 359, Trp 391, Tyr 394, Lys 268, Phe 309, Trp 351, and Cys 358. This manifests the crucial role of these amino acids in boosting activity. Thus, it can be stated that the presence of these amino acids is necessary for the inhibition of MAO-A. Based on the molecular docking results, the predicted compounds (Pred 1-7) can be effective in treating behavioral problems, especially depression.

CONCLUSIONS

In this study, virtual screening studies, including 3D-QSAR, ADMET properties, and molecular docking, were applied to a number of 2-acetylphenol-rivastigmin hybrids as MAO-A inhibitors. PLS approach and CoMSIA revealed strong correlative and predictive abilities (r^2 = 0.904, q^2 = 0.699, and SEE = 0.094) using the following descriptors:

Table 4. Lipinski's Rule of 5 of New Compounds and the Template in the Data Set

Mol	Property				
	Molecular weight	logP	Rotatable bonds	H-bond acceptor	H-bond donor
Rule	< 500	< 5	< 10	< 10	< 5
3E	239.29	1.820	2	4	1
Pred1	224.21	0.551	2	4	2
Pred2	241.20	0.40	3	6	4
Pred3	256.21	0.019	3	6	4
Pred4	342.41	2.602	4	6	3
Pred5	326.41	2.814	7	5	3
Pred6	300.33	1.576	3	6	3
Pred7	314.36	1.967	7	6	3

Table 5. ADMET Prediction of New Molecules and the Template 3E in the Data Set

Comp	Absorption			Distribution	Metabolism						Excretion	Toxicity		
	water solubility	CaCO2 permeability	intestinal absorption human	blood-brain barrier	CYP						total clearance	AMES toxicity	carcino-mouse	Hepato-Toxicity
					2D6	3A4	2C19	2C9	2D6	3A4				
					Substrate		Inhibitor							
	Numeric (logM)	Numeric (log Papp in $10\text{-}6$ cm s^{-1})		Numeric (logBB)	Categorical (yes/no)						Numeric (log ml/min/kg)	categorical (yes/no)		
3E	-2.635	22.89	96.75	0.027	No	No	No	No	No	No	0.208	No	No	No
Pred 1	-1.99	21.1	81.92	0.365	No	No	No	No	No	No	0.691	No	No	No
Pred 2	-1.75	20.12	58.899	0.028	No	No	No	No	No	No	0.267	No	No	No
Pred 3	-1.89	20.06	55.86	0.03	No	No	No	No	No	No	0.621	No	No	No
Pred 4	-2.788	21.03	87.42	0.078	No	No	No	No	No	No	-0.08	No	No	No
Pred 5	-2.524	21	90.09	0.151	No	No	No	No	No	No	0.174	No	No	No
Pred 6	-2.16	20.93	83.28	0.032	No	No	No	No	No	No	-0.149	No	No	No
Pred 7	-2.479	20.6	84.93	0.062	No	No	No	No	No	No	0.122	No	No	No

Table 6. A Comparison of Pred1-7 Designed Molecules and the Reference Drug Based on Their Molecular Docking Values and Binding Interactions with the MAO-A

Compounds	Binding affinity (kcal mol^{-1})	Number of hydrogen interactions	Other interactions
3E	-7,9	3 Arg33, Met395, gly32	2 Arg33, Ala398
Pred1	-7,9	3 Arg33, Met395, Tyr359	2 Arg33, Ala398
Pred2	-8,1	7 Arg33, Arg28, Glu26, Gly7, Ile8, Gly32, Ser9	-
Pred3	-8,4	4 Arg28, Glu26, Ile8, Ser9	-
Pred4	-9,7	2 Arg33, gly32	3 Arg33, Ala398, Tyr359
Pred5	-7,9	4 Tyr50, Asn155, Tyr394, Met395	4 Tyr359, Trp391, Tyr394
Pred6	-8,7	2 Arg33, gly32, Thr34	4 Arg33, Ala398, Tyr359, tyr394
Pred7	-8,6	3 Arg33, Met395, gly32	7 Arg33, Ala398, Lys268, Phe309, Trp351, Tyr359 Cys358

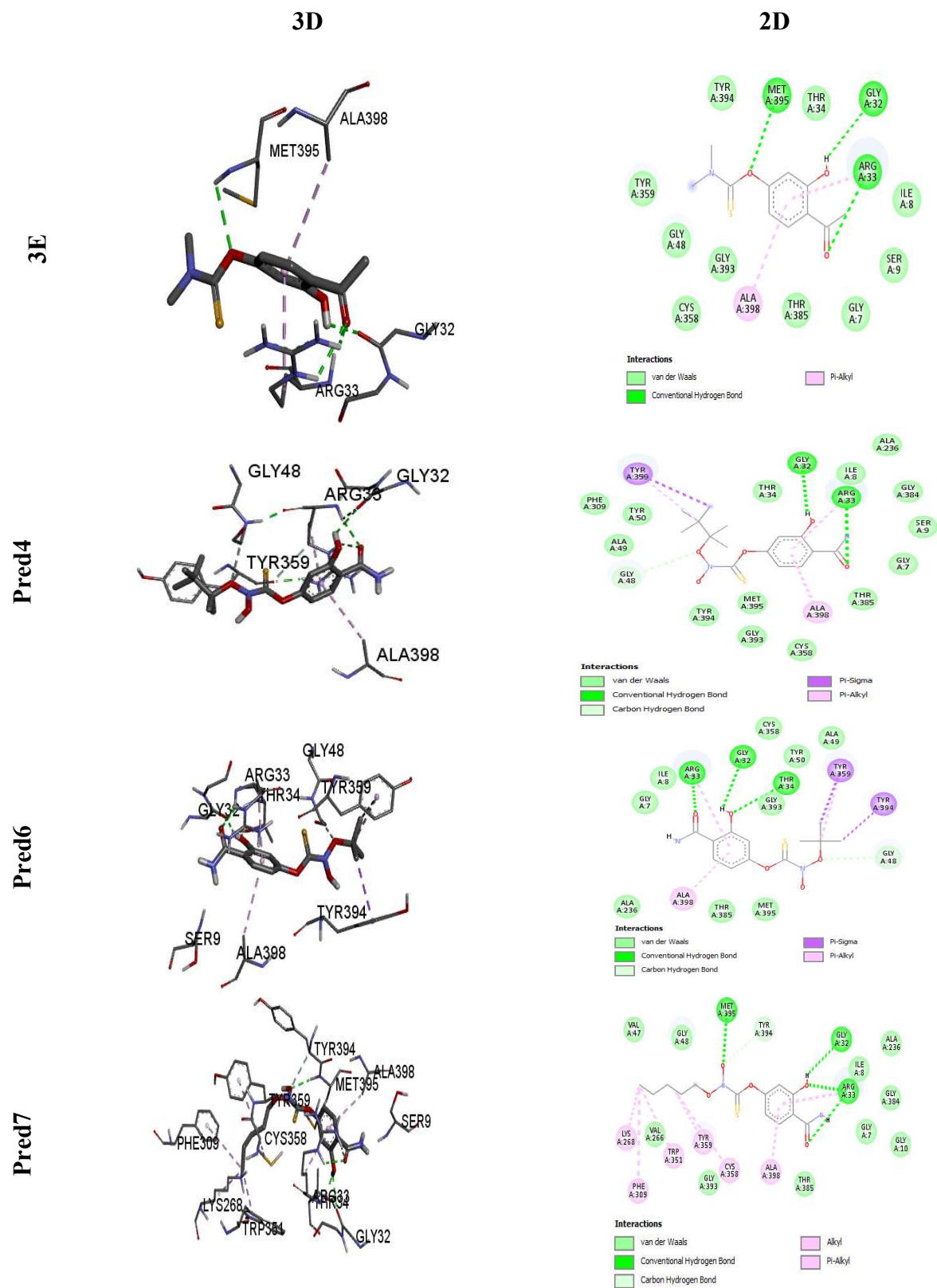**3D**   **2D**

Fig. 6. 2D and 3D interactions of ligand 3E and the predicted compounds.

steric field, electrostatic field, hydrophobic field, and hydrogen-bond acceptor field. The pharmacokinetic characteristics of the designed compounds (Pred1-Pred7) were also studied using drug similarity and ADMET prediction. Molecular docking was performed to study the interactions between the ligands and the MAO-A receptor at the active site of the receptor. Finally, the interactions between the MAO and the predicted compounds showed that the designed compounds had the potential to be promising candidates for the treatment of depression.

REFERENCES

[1]   Shih, J. C., *et al.*, Monoamine oxidase: From genes to behavior, *Annu. Rev. Neurosci.*, **1999**, *22*, 197-217, DOI: 10.1146/annurev.neuro.22.1.197.

[2]   Kochersperger, L. M., *et al.*, Assignment of genes for human monoamine oxidases A and B to the X chromosome, *J. Neurosci. Res.*, **1986**, *16* (4), 601-616, DOI: 10.1002/jnr.490160403.

[3]   Bach, A. W., *et al.*, cDNA cloning of human liver monoamine oxidase A and B: molecular basis of differences in enzymatic properties., *Proc. Natl. Acad. Sci. U. S. A.*, **1988**, *85* (13), 4934-4938, DOI: 10.1073/pnas.85.13.4934.

[4]   Zisook, S., A clinical overview of monoamine oxidase inhibitors, *Psychosomatics*, 1985, *26* (3), 240-246, DOI: 10.1016/S0033-3182(85)72877-0.

[5]   El Aissouq, A., *et al.*, Computational investigation of unsaturated ketone derivatives as MAO-B inhibitors by using QSAR, ADME/Tox, molecular docking, and molecular dynamics simulations, **2022**, *46* (3).

[6]   Shalaby, R., *et al.*, SAR and molecular mechanism studies of monoamine oxidase inhibition by selected chalcone analogs, *J. Enzyme Inhib. Med. Chem.*, **2019**, *34*, 1, 863-876, DOI: 10.1080/14756366.2019.1593158.

[7]   Kumar, B., *et al.*, 4,6-Diphenylpyrimidine Derivatives as Dual Inhibitors of Monoamine Oxidase and Acetylcholinesterase for the Treatment of Alzheimer's Disease, *ACS Chem. Neurosci.*, **2019**, *10* (1), 252-265, DOI: 10.1021/acschemneuro.8b00220.

[8]   lhan Turan-Zitouni, G., *et al.*, Design, synthesis and biological evaluation of novel n-pyridyl-hydrazone

derivatives as potential monoamine oxidase (MAO) inhibitors, *Molecules*, **2018**, *23* (1), DOI: 10.3390/molecules23010113.

[9]   Larit, F., *et al.*, Inhibition of human monoamine oxidase A and B by flavonoids isolated from two Algerian medicinal plants, **2018**, *40*, DOI: 10.1016/j.phymed.2017.12.032.

[10] Lee, H. W., *et al*., Potent selective inhibition of monoamine oxidase a by alternariol monomethyl ether isolated from alternaria brassicae, *J. Microbiol. Biotechnol.*, **2017**, *27* (2), 316-320, DOI: 10.4014/jmb.1610.10053.

[11] Sang, Z., *et al.*, Multifunctional scutellarin-rivastigmine hybrids with cholinergic, antioxidant, biometal chelating and neuroprotective properties for the treatment of Alzheimer's disease, *Bioorganic Med. Chem.*, **2015**, *23* (4), 668-680, DOI: 10.1016/j.bmc.2015.01.005.

[12] Xiao, G., *et al.*, Design, synthesis and biological evaluation of 4'-aminochalcone-rivastigmine hybrids as multifunctional agents for the treatment of Alzheimer's disease, *Bioorganic Med. Chem.*, **2017**, *25* (3), 1030-1041, DOI: 10.1016/j.bmc.2016.12.013.

[13] Nesi, G., *et al.*, Nature-based molecules combined with rivastigmine: A symbiotic approach for the synthesis of new agents against Alzheimer's disease, *Eur. J. Med. Chem.*, **2017**, *141*, 232-239, DOI: 10.1016/j.ejmech.2017.10.006.

[14] Zhu, G., *et al.*, The development of 2-acetylphenol-donepezil hybrids as multifunctional agents for the treatment of Alzheimer's disease, *Bioorganic Med. Chem. Lett.*, **2019**, *29* (19), 126625, DOI: 10.1016/j.bmcl.2019.126625.

[15] Sang, Z., *et al.*, Apigenin-rivastigmine hybrids as multi-target-directed liagnds for the treatment of Alzheimer's disease, *Eur. J. Med. Chem.*, **2020**, *187*, 111958, DOI: 10.1016/j.ejmech.2019.111958.

[16] Vicente-zurdo, D., *et al.*, Novel Rivastigmine Derivatives as Promising Multi-Target Compounds for Potential Treatment of Alzheimer's Disease, *Biomedicines*, **2022**, *10* (7), 1-27, DOI: 10.3390/biomedicines10071510.

[17] Devillers, J., *Juvenile hormones and juvenoids: Modeling biological effects and environmental fate.*

2013, DOI: 10.1201/b14899.

[18] El Rhabori, S., *et al*., QSAR, molecular docking and ADMET studies of quinoline, isoquinoline and quinazoline derivatives against Plasmodium falciparum malaria, *Struct. Chem.*, **2022**, 0123456789, DOI: 10.1007/s11224-022-01988-y.

[19] Tabti, K., HQSAR, CoMFA, CoMSIA docking studies and simulation MD on quinazolines/quinolones derivatives for DENV virus inhibitory activity, **2022**.

[20] Laoud, A., *et al*., Identification of novel nt-MGAM inhibitors for potential treatment of type 2 diabetes: Virtual screening, atom based 3D-QSAR model, docking analysis and ADME study, *Comput. Biol. Chem.*, **2018**, *72*, 122-135, DOI: 10.1016/j.compbiolchem.2017.12.003.

[21] Laoud, A., *et al*., Discovery of New Inhibitors of Enoyl-ACP Reductase *via* Structure-Based Virtual Screening, *Phys. Chem. Res.*, **2023**, *11* (3), 459-469, DOI: 10.22036/pcr.2022.342259.2106.

[22] El Mchichi, L., *et al*., Molecular Docking, Drug likeness Studies and ADMET prediction of Flavonoids as Platelet-Activating Factor (PAF) Receptor Binding, **2021**, *4*, 145-152.

[23] El McHichi, L., *et al.*, *In silico* design of novel Pyrazole derivatives containing thiourea skeleton as anti-cancer agents using: 3D QSAR, Drug-Likeness studies, ADMET prediction and molecular docking, *Mater. Today Proc.*, **2021**, *45*, 7661-7674, DOI: 10.1016/j.matpr.2021.03.152.

[24] Ferreira, L. G., *et al*., *Molecular docking and structure-based drug design strategies*, **2015**, *20* (7), DOI: 10.3390/molecules200713384.

[25] Deng, C., *et al.*, Design, synthesis, and biological evaluation of novel 2-acetylphenol-rivastigmine hybrids as potential multifunctional agents for the treatment of Alzheimer's disease, *Med. Chem. Res.*, **2022**, *31* (6), 1035-1048, DOI: 10.1007/s00044-022-02899-7.

[26] Tong, *et al*, Quionolone carboxylic acid derivatives as HIV-1 integrase inhibitors: Docking-based HQSAR and topomer CoMFA analyses, *Physiol. Behav.*, **2017**, *176*, 5, 139-148, DOI: 10.1002/cem.2934.Quionolone.

[27] Caballero, J., *et al*., Quantitative structure-activity relationship of rubiscolin analogues as δ opioid peptides using comparative molecular field analysis (CoMFA) and comparative molecular similarity indices analysis (CoMSIA), *J. Agric. Food Chem.*, **2007**, *55* (20), 8101-8104, DOI: 10.1021/jf071031h.

[28] Klebe, G., *et al*., Molecular Similarity Indices in a Comparative Analysis (CoMSIA) of Drug Molecules To Correlate and Predict Their Biological Activity, *J. Med. Chem.*, **1994**, *37* (24), 4130-4146, DOI: 10.1021/jm00050a010.

[29] Wu, S., *et al*., CoMFA and CoMSIA analysis of ACE-inhibitory, antimicrobial and bitter-tasting peptides, *Eur. J. Med. Chem.*, **2014**, *84*, 100-106, DOI: 10.1016/j.ejmech.2014.07.015.

[30] Pireset, D. E. V. *et al*., pkCSM: Predicting small-molecule pharmacokinetic and toxicity properties using graph-based signatures, *J. Med. Chem.*, **2015**, *58* (9), 4066-4072, DOI: 10.1021/acs.jmedchem.5b00104.

[31] A. J. O. OLEG TROTT, Software News and Update AutoDock Vina: Improving the Speed and Accuracy of Docking with a New Scoring Function, Efficient Optimization, and Multithreading, *J. Comput. Chem.*, **2009**, 455-461, DOI: 10.1002/jcc.